Journal of Geophysical Research: Atmospheres

RESEARCH ARTICLE
10.1029/2018JD028357

Optical Properties and Spatial Variation of Tropical Cyclone Cloud Systems From TRMM and MODIS in the East Asia Region: 2010–2014

Yiwen Zhou[1,2], Yong Han[1,2], Yonghua Wu[3], Tijian Wang[2], Xiaodong Tang[2,4], and Yuan Wang[2,4]

[1]Guangdong Province Key Laboratory for Climate Change and Natural Disaster Studies, School of Atmospheric Sciences, Sun Yat-sen University, Guangzhou, China, [2]School of Atmospheric Sciences, Nanjing University, Nanjing, China, [3]NOAA-CREST, City College of New York, New York, NY, USA, [4]Key Laboratory of Mesoscale Severe Weather of Ministry of Education, School of Atmospheric Sciences, Nanjing University, Nanjing, China

Key Points:
- The optical properties and spatial distributions of 35 tropical cyclone cloud systems (TCCS) in East Asia are analyzed
- The regress equations and an ideal fitting model along the radial distance to TC center have been constructed
- The relationship of clouds and precipitations with aerosol optical thickness (AOT) is verified

Correspondence to:
Y. Han,
hanyong@nju.edu.cn;
hany66@mail.sysu.edu.cn

Citation:
Zhou, Y., Han, Y., Wu, Y., Wang, T., Tang, X., & Wang, Y. (2018). Optical properties and spatial variation of tropical cyclone cloud systems from TRMM and MODIS in the East Asia region: 2010–2014. *Journal of Geophysical Research: Atmospheres*, *123*, 9542–9558. https://doi.org/10.1029/2018JD028357

Received 20 JAN 2018
Accepted 6 AUG 2018
Accepted article online 15 AUG 2018
Published online 2 SEP 2018

Abstract The tropical cyclone (TC) in East Asia varies strongly each year, indicating the different spectral characteristics of the TC cloud systems (TCCSs) with the distance from the center of TC. We report a new perspective of optical properties of TCCS by using the Moderate Resolution Imaging Spectroradiometer and Tropical Rainfall Measuring Mission data over the years from 2010 to 2014 for the 35 TCs in East Asia. We investigate the spatial distribution of the cloud-top height, radar reflectivity, polarization corrected temperature in 85.5 GHz ($PCT_{85.5}$), hydrometeor vertical profile, cloud water path, cloud optical thickness, and cloud particle effective radius of TCCS in the development, maturity, and decay stages of TC. The results indicate the significant differences of cloud characteristics in the maturity stage in comparison to other two stages, showing the higher radar reflectivity up to 30 dBZ and the $PCT_{85.5}$ as low as 232.98 K in the TC eye wall. Meanwhile, the mean hydrometeor profile indicates more ice particles accumulating above the height of 10 km but less liquid droplets near 3 km. The peak of cloud water path and cloud optical thickness in the maturity stage can reach to 1,300 g/m^2 and 75, respectively. The mean cloud particle effective radius and precipitation in the three stages could be influenced by aerosols. Based on these quantified results, several ideal fitting equations and the models are constructed to denote the properties of TCCS. Two cases are analyzed to examine the accuracy of the quantified mean state for different stages of TCCS and the relationship between aerosols and clouds.

1. Introduction

Tropical cyclones (TCs) are the most deadly storms on earth, and the intense TCs are capable of producing catastrophic loss of lives and property damage to coastal residents around the world (Chang et al., 2012; Yonekura & Hall, 2014), especially in East Asia (Chan & Kepert, 2010). And the TC cloud system (TCCS) is also a key factor in climate modulation system (Balaguru et al., 2014; Mei et al., 2013; Sriver & Huber, 2007). As a large-scale cloud system, it reflects the shortwave radiation from the sun and emits the long-wave radiation, which controls the fluctuation of atmospheric temperature (Koh & Fonseca, 2015; Pithan et al., 2014; Stephens & Wong, 1987). Also, from a climate dynamic standpoint (Li et al., 2010), TCCS is particularly important for the accurate representation of numerical simulations for the cloud distribution and radiation globally (Houze, 2010).

TCs often form from the tropical warm ocean, where the traditional observation data from buoys, ships, and surface-based stations are sparse (Montgomery & Farrell, 1993). In the past decades, due to the development of space technology and satellite remote sensing, the satellites are more suitable methods for studying large scale of TCCS surveillance than other observation means. Cloud dynamic structure and precipitation with a broader spatial and temporal distribution can be investigated by a systematic examination method (Matveev, 1999). The satellites can provide a temperature and moisture vertical profile through a deep cloud system from visible, infrared band to microwave band. For example, Special Sensor Microwave Imager, Tropical Rainfall Measuring Mission (TRMM), and Moderate Resolution Imaging Spectroradiometer (MODIS) could provide a variety of technical support for studying TCCS macroscopic and microphysical characteristics, which is critical for TCCS short-term forecast and intensity analysis (Liu et al., 2008; Marchand et al., 2010; Tourville et al., 2015).

Consequently, previous researches have been conducted on the satellite application in intensity, dynamic, thermodynamic, or precipitation of the TCCS (Balaguru et al., 2014; Haig & Nott, 2016; Wing et al., 2015). Chao et al. (2011) made use of both infrared and visible satellite images to estimate the TC rotation and wind speed. Lau et al. (2008) utilized the TRMM rainfall data to study the relationships between TC and extreme rain events. In addition, the TCCS optical characteristics are important factors for understanding the role of TCCS in the Earth's radiation budget, for example, cloud optical thickness (COT) and cloud particle effective radius (CER; King et al., 2004; Szczodrak et al., 2001; Nakajima & King, 1990). Nakajima and King (1990) described that the COT and CER can be determined from a water-absorbing channel in the near-infrared wavelength and a nonabsorbing channel in the visible wavelength. And, a well-behaving inversion algorithm can be applied to compute cloud optical properties in the satellite-based measurement (Bennartz, 2007; Wood et al., 2008).

Aerosol effects on clouds could further extend to precipitation, through the formation, development, and decay of clouds, therefore, it is essential to master the microphysical process of aerosols on clouds (Rosenfeld et al., 2012; Wang, Lee, et al., 2014). Prior study of aerosol indirect effect has confirmed that one of the major influence factors is that enhanced aerosol content can suppress the precipitation by reducing the particle size (Squires & Twomey, 1960). Furthermore, Albrecht (1989) found that the increasing of aerosol concentration may reduce the size of cloud droplets and the precipitation may be shut off or delayed. And aerosol invigoration effect on convective cloud system for thunderstorms (Wang et al., 2011) and extra-TCs (Wang, Fu, et al., 2014) have also been elucidated carefully. There are ample pieces of evident of aerosol indirect effects from in situ, remote sense, and ground-based observations (Lin et al., 2010; Min et al., 2008, 2012). Remote sensing of aerosol concentration and size parameters from satellite is also essential to the contribution of the aerosol radiative forcing on the cloud climate change. The aerosol product derived from MODIS is continuously being evaluated with ground-based measurements at global, regional, and local scales and at different time scales in previous studies (Kahn et al., 2007; Li et al., 2007; Zhang & Reid, 2006). And absorbing aerosols could seriously affect COT, rain rate, and liquid water content retrievals from both remote sensing measurements (Li et al., 2011, 2014). In remote sensing data set, research progress in the aerosol product in the vicinity of clouds is essential to help us separate the aerosol and cloudy pixels. In the assumption that most cloudy pixels exhibit larger spatial variability than the aerosols, passive remote sensors distinguish the signals between them. The aerosol observation near the cloud edge was retrieved by aggregating the reflectance from six channels at 553, 664, 855, 1,243, 1,623 and 2,199 nm (Martins et al., 2002), respectively. The standard deviation of 553 nm reflectance is compared to the threshold of 0.0025. If it is larger than 0.0025, the pixel is declared *cloudy* (Martins et al., 2002). The experiments conducted by Redemann et al. (2009) show an increase of 20% in aerosol optical thickness (AOT) in the proximity of clouds due to the humidity increasing. Ichoku et al. (2004) suggested that MODIS aerosol products have been proven useful and accurate for estimating the regional aerosol radiative forcing both at the top of the atmosphere and close to the surface. Generally, the integration of TCCS with aerosol process obtained from the satellite sensors is a powerful tool and provides under great opportunity to address this issue.

A number of foregoing studies have examined the characteristics for a single TCCS or case study (Han et al., 1998; Kidder et al., 2009; Nesbitt et al., 1999). To our best knowledge, there is lack of the statistical spatial distribution characteristics with the distance from the center of TC on optical properties, such as the radar reflectivity, $PCT_{85.5}$, cloud water path (CWP), COT, and CER, as well as their variability in the TCCS development, maturity, and decay stages, combined by multiple TCs in East Asia. Satellite imagery is often used to estimate structure and intensity or the characteristics of single TC (the previous detailed research progress is listed in Table 1), but the synergistic use of satellite data set can help further understand TC life cycle. In this study, we analyze the cloud spectral structure information of TCCS based on the data set from TRMM and MODIS; 35 TC events landing in East Asia during 2010 to 2014 are investigated. The aim of this present study is to understand the spatial distribution and optical properties of TCCS through 5 years satellite data and to build a relationship or ideal fitting equations for the spatial variability. The quantification of the TC cloud spectrum will add our knowledge of the diversity of cloud and the complexity of the microphysical processes and finally optimize the TC forecasting process. To better understand the effects of aerosol on clouds, especially on the convective clouds, we select a TC case for further analysis. Correlations between aerosol effective radius (AER) and CER from the MODIS are examined along the track of TC. The layout of the paper is as follows. In section 2, a brief description of the valid data set and methodology is given. Section 3 presents and

Table 1
Cloud Optical Properties Detected by Satellite in Other Investigations

Instrument	Research priority	TC	References
TRMM	Vertical wind shear storm motion	All TCs from 1998 to 2000	Chen et al. (2006)
ISCCP	Temporal and spatial distribution	All TCs from 1983 to 2005	Knapp and Kossin (2007)
MODIS	Brightness temperature COT CWP	An extratropical cyclone in the North Atlantic Ocean	Otkin and Greenwald (2008)
TRMM	Rain band characteristics	TCs from 1993 to 2007	Yokoyama and Takayabu (2008)
CloudSat	Cloud classification	Prapiroon(2006)	Durden et al. (2009)
A-train	Cloud water products Cloud ice products	Ileana(2006)	
FY-3B	Ice water path	Muifa(2011)	Wang, Fu, et al. (2014)
MODIS	Brightness temperature	Merbok(2011)	
AMSU-A	Cloud fraction	Sandy(2012)	Han et al. (2016)
MODIS	Brightness temperature	Haiyan(2013)	
Suomi-NPP	COT		

Note. TC = tropical cyclone; TRMM = Tropical Rainfall Measuring Mission; MODIS = Moderate Resolution Imaging Spectroradiometer; COT = cloud optical thickness; CWP = cloud water path.

discusses the observation results from satellites. We focus on the variation of TCCS characteristics in this work. Two cases are also proposed to analyze the interaction between cloud and aerosols, and due to the complexity of the interaction, two case studies are not enough to reveal the mechanism, so this part has not been overemphasized in this paper. And conclusions and summary are shown in section 4.

2. Data and Methods

To illustrate the spatial distribution of optical properties on TCCS, we first select 35 case studies of TC. Next, to generalize the results, we analyze the observed TC data from MODIS and TRMM satellites, focusing on the spatial variation along the distance from the center of TC on optical properties of TCCS, such as the radar reflectivity, $PCT_{85.5}$, CWP, COT, and CER at TCCS in development, maturity, and decay stages. More details are provided in the subsections below.

2.1. Satellite Products

The satellite products from NASA TRMM (Iguchi et al., 2000; Olson et al., 2000) and MODIS are used (Platnick et al., 2003). The TRMM houses four functioning instruments (Kummerow, 2000), including the precipitation radar, Microwave Imager (TMI), Lightning Image Sensor, and Visible and IR Scanner. The precipitation radar looks through the precipitation column and provides new insights into tropical storm (TS) structure and intensification. The TRMM TMI measures the microwave energy emitted from the Earth, and then quantifies the water vapor, the cloud water, and the rainfall intensity in the atmosphere. The TMI has a 760-km swath width with horizontal resolution of 5 × 7 km. It can obtain the information on the vertically integrated ice and water path. Although the wavelength at 85.5 GHz is more sensitive to the reflection of ice particles, however, there are some ambiguities from the combination of scattering and absorption effects at this wavelength (85.5 GHz), especially it is difficult to objectively distinguish regions of dry clear air from cold-cloud precipitation over the ocean. In order to eliminate the error, the polarization-corrected temperature at 85.5 GHz ($PCT_{85.5}$) was given by Spencer et al. (1989) as follows, $PCT_{85.5} = 1.818T_{BV85.8} - 0.818T_{BH85.5}$, which combines 85.5 GHz horizontal polarization channel $T_{BH85.5}$ with vertical polarization channel $T_{BV85.5}$ value. It removes the contrast in brightness temperature over land versus ocean. The ice-scattering signals are retained, so the depression of $PCT_{85.5}$ directly reflected the vertically integrated ice water path.

The MODIS instruments are on-aboard the Terra and Aqua satellites (Boeke et al., 2016; Platnick et al., 2003), respectively, which can provide global observations of Earth's land, oceans, and atmosphere in the visible and infrared regions of the spectrum. The Level 2 products on cloud (MOD 06) and aerosol (MOD 04) of MODIS are selected in this study, and the products include the brightness temperature, cloud height, COT, CER, CWP, AOT and AER (Menzel et al., 2015; Platnick et al., 2015). The COT is a key parameter that reflects the characteristics of cloud radiation properties through the vertical integration of the extinction

Table 2
The Intensity of TC Classification

Intensity classification	Maximum surface wind near TC center (m/s)	Abbreviations
Tropical depression	10.8–17.1	TD
Tropical storm	17.2–24.4	TS
Severe tropical storm	24.5–32.6	STS
Typhoon	32.7–41.4	TY
Severe typhoon	41.5–50.8	STY
Super typhoon	>50.8	Super TY

Note. TC = tropical cyclone.

coefficients. It is closely related to the CWP in the TCCS. AOT represents the extinction of incoming solar radiation by aerosols through the whole atmospheric column. CER and AER are the mean cloud and aerosol particle size. All of them are the key parameters in the atmospheric water circulation and Earth's radiative energy balance study.

2.2. Methods

In Table 2, we show six categories of TC according to the intensity classification standard of China Meteorology Administration (Ying et al., 2014; http://tcdata.typhoon.gov.cn). The life cycle of each TC can be divided into three stages: development, maturity, and decay stage. The development stage is defined from the TC generation to the Severe TS (STS). The maturity stage is defined as the intensity being in or surpassing Typhoon (TY). The extinction stage is defined from the TC weaken to extinction.

About the TC's radial range, Larson et al. (2005) suggested that 550 km could be a threshold of TC raining area from the historical statistical data investigation. Englehart and Douglas (2001) also found that there are about 90% TC cases' radius less than 550–600 km from the center of a storm to the outer edge TCCS. In different stages, there are remarkable correlation between the scale and intensity of TC (Lu et al., 2011). Overall, a truncation of 500 km could reflect the mean state characteristics of TCs to some degree. After we analyzed the average maximum wind radius of TS, STS, and TY 30 kt from 1977 to 2015 in East Asia, there are 267.929, 389.910, and 487.764 km, respectively. Based on these facts, we define that the TC radial range is less than 500 km in East Asia.

We select 35 TCs (Figure 1) landfalling in China from 2010 to 2014 from the RSMC Tokyo-Typhoon Center [http://www.jma.go.jp/ and http://tcdata.typhoon.gov.cn]. Because there are some differences between the record time and the overtime of TRMM and MODIS, we use the linear interpolation to determine the exact intensity and the eye location of each TC. We finally achieved 434 orbits of TRMM data sets (version 6) including 1B11, 2A12, and 2A25. And at the same time, there are 294 orbit MODIS data including MOD06 cloud products within ±2 hr when TRMM passed by East Asia region. There are 227, 102, and 105 orbit data for the development, maturity, and decay stage of TCCS from TRMM satellite, respectively. Meanwhile, we get 157, 63, and 74 orbit data for those TCCS from MODIS, respectively.

3. Results and Discussion

3.1. The Structure of TCCS

We begin with the statistical analysis of 35 TCCS cases in East Asia during 2010 to 2014. Houze (2010) indicated that the TCs can be divided into three components in horizontal direction as follows: the TC eye, the

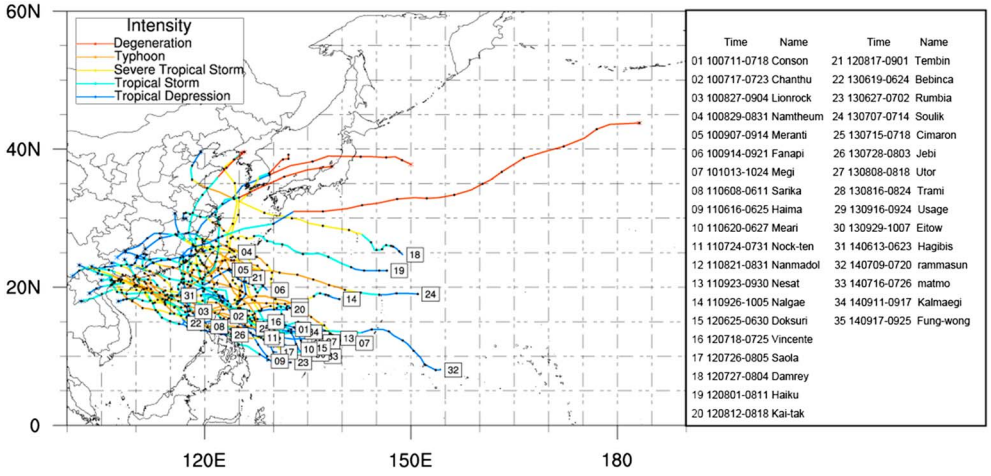

Figure 1. The 35 landfilling tropical cyclones in China during the period from 2010 to 2014 recorded by RSMC Tokyo-Typhoon Center.

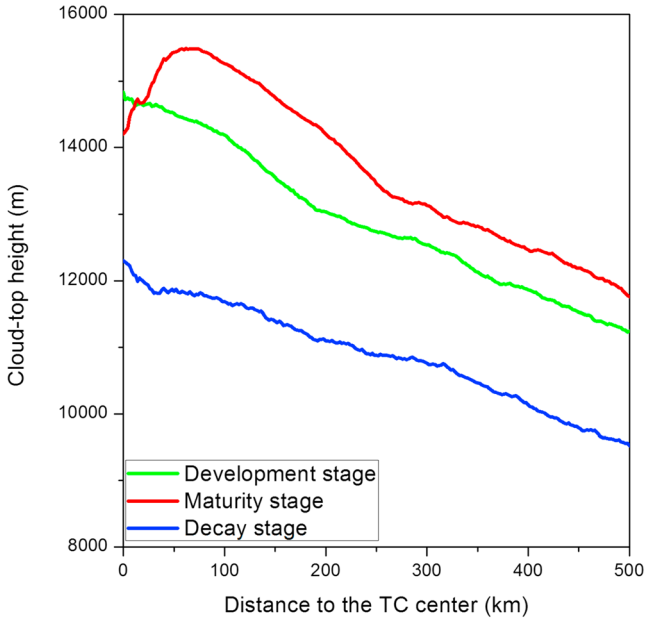

Figure 2. The averaged cloud-top height derived from the Moderate Resolution Imaging Spectroradiometer MOD06 products for the 35 TCs in the development, maturity, and decay stages in East Asia, respectively. TC = tropical cyclone.

cloud eye wall, and the spiral cloud-rain band. The TC eye is usually near the center of a mature TCCS with just little rain and free of clouds, where air sinks rather than rises. The cloudy outer edge of the eye is a convective cell called the *eye wall*, where the greatest wind speeds are found, air rises most rapidly, clouds reach to their highest altitude, and precipitation is the heaviest. Outside the eye wall, the extensive region of spiral cloud-rain band can be found.

Knowledge of cloud properties like cloud-top height (CTH) is essential to understand their impact on Earth's radiation effect. To compare the CTH in different stages directly, Figure 2 shows the average CTH for the 35 cases calculated from MODIS product. In general, the CTH is expected to reduce with the increasing distance to the TC eye, except within the range of 100 km in the maturity stage. For the decay stage, the average CTH is about 2 km lower than that of development stage. And for the development stage, the average CTH is 1 km lower than that of maturity stage. As we know, a well-defined eye is one of the most remarkable features of a mature TC, where mostly calm weather occurs. The eye is always clear or has low-level clouds. Therefore, the CTH for maturity stage in TC eye is lower than that in eye wall region. Although the CTH for three stages is different, the descending gradient for three stages does not change greatly.

In order to study the inner structure characteristics of TCCS, Figures 3a–3c present the radar reflectivity in three different stages above ground level to the altitude of 10 km by the TRMM 2A25 data, which is mainly related to the particle or droplet phase and size distribution of cloud. The statistical differences show that the relationships between the radar reflectivity and TC intensity are as follows: In the development and maturity stage, the obvious existence of TC eye slightly reduces the mean radar reflectivity close to the center core. But, it rises up quickly in the eye wall because of the small size of the eye compared to the whole cloud system. In decay stage, there is no remarkable feature of TC eye. We can also clearly see that the area of intensified radar reflectivity ($\geq$28 dBZ) in maturity stage is twice or more than the one at other two stages in horizontal direction. A wider extension range will reach up to near 200 km away from the TC center in maturity stage, around 180 km in development stage, and 100 km in decay stage. Meanwhile, most radar reflectivity in maturity stage can exceed 30 dBZ, which covers a considerable area near the eye wall. The occurrence of higher radar reflectivity thresholds in this stage illustrates that convective activities can be promoted significantly with the increasing intensity. The height with the maximum echo is always concentrated near 5 km, which suggests the influence of the bright band at this height. At the height of 5–6 km, the radar reflectivity decreases to 24 dBZ for the ice water mixed layer. Previous research has been conducted that the depth of mixed layer was concerned with the water vapor mixing ratio and the temperature, which could cause a sharp decrease in the radar reflectivity (Heinselman et al., 2009; Heymsfield et al., 1999). Meanwhile, above 6 km of the ice layer, the increasing of ice particle content leads to the water vapor content quickly depresses to 20 dBZ. In the spiral cloud-rain band, a small quantity of large radar reflectivity can be observed. The average radar reflectivity drops to 25 dBZ. However, there still exists a little large echo near 1–2.5 and 4–5 km, respectively. The radar reflectivity distinctions among the three stages indicate that the intensity of TCs shows much influence of genesis and destruction in the cloud systems. When predicting the intensity, the radar reflectivity presented above suggests the rule that the stronger stage the TC is, the larger radar reflectivity is, especially within the range of eye wall. It probably reflects that the more convective core and complex microphysical process frequently occur in this region.

3.2. The Optical Parameters Spatial Variation of TCCS

Figure 4 shows the radial variation of average $PCT_{85.5}$ derived from TRMM 1B11 products, and the three different color curves represent the development stage, maturity stage, and decay stage, respectively. In order to avoid the influence of land or ocean surface, all the sample points of $PCT_{85.5} \geq 273$ K are ignored. From Figure 4a, we find that the average values of $PCT_{85.5}$ are almost between 230 and 260 K in all stages.

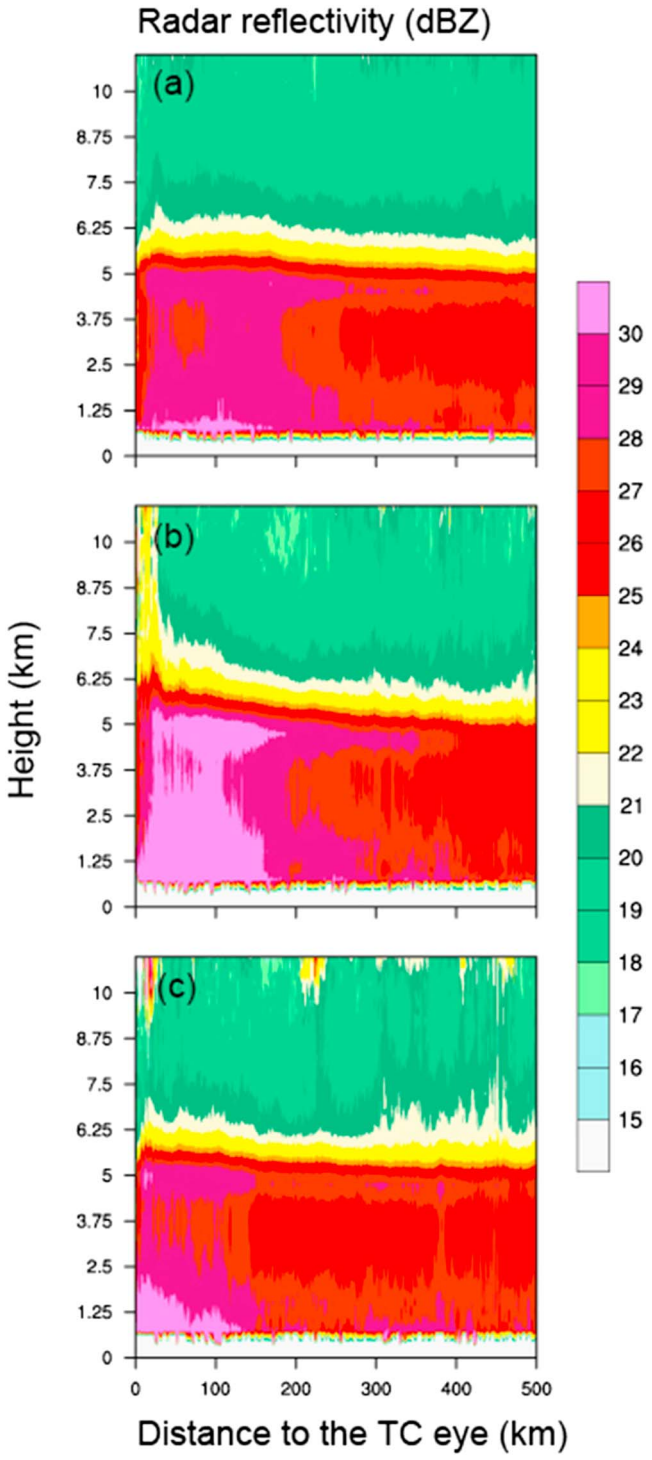

Figure 3. The average radius-height sections of radar reflectivity (units: dBZ) derived from Tropical Rainfall Measuring Mission 2A25 products of 35 TCs in (a) development stage, (b) maturity stage, and (c) decay stage of TC cloud system in East Asia, respectively. TC = tropical cyclone.

However, there is still some significant difference in radial variation among them, especially within the range of 100 km. In general, the mean $PCT_{85.5}$ in the decay stage is 7–8 K higher than that in development stage and 15–20 K higher than maturity stage in the eye wall region. While the most obvious change appears in the maturity stage, the $PCT_{85.5}$ decreases first and followed by a sharp increase in this stage near the TC eye, where the most particles have a lower $PCT_{85.5}$ value than that of others. This feature in the TC eye also appears in development stage and decay stage, but less obvious than that of maturity stage. The minimum $PCT_{85.5}$ values at three stages are 244.78, 232.98, and 251.22 K appearing near 42, 26, and 30 km, respectively, which reflects that, in maturity stage, there are a pronounced ice scattering signature and tighter structure for TCCS. In the distance of 100–500 km from the center of TC, the mean $PCT_{85.5}$ in the extinction stage still maintains the highest value. The lines of development and maturity stage tend to overlap, because the cloud cover becomes scarce away from the center or the TCCS would be affected by other weather systems.

Figures 4b–4d are the $PCT_{85.5}$ distribution within 500 km; we only show the lowest 5% to mean percentile of the whole distribution in the consideration of only the low value of $PCT_{85.5}$ having the profound physical meaning. The upper limit of it, which reflects the mean distribution of $PCT_{85.5}$, has been discussed above. These pictures also indicate that 85% of pixel points are located above temperatures of 220 K, except for that of the 100 km from the TC eye in maturity stage. The closer to the storm center, the lower the probability that $PCT_{85.5}$ exists. In the development (Figure 4b) and extinction stage (Figure 4d), only few pixels reveal the $PCT_{85.5}$ under 200 K. The $PCT_{85.5}$ can provide information about the vertical distribution of the hydrometers within the TCCS. Under this condition, there is lower $PCT_{85.5}$ for most cloud particles in maturity stage than that of the other two stages, attributed to the ice scattering within deep convection and precipitating anvil clouds. The results above indicate that the content of ice particles is relatively small in the development and decay stage. With the development of TCs, the $PCT_{85.5}$ decreases sharply within 100 km from the TC center in maturity stage, which reflects that the content of ice particles relatively increase in the eye wall.

In order to understand hydrometeor in the TCCS, we analyzed the variability of cloud liquid and ice water in vertical distribution. Figure 5 shows the results at the three different stages of TC. The greatest variability was near the troposphere at the height of 9–13 km for the cloud ice water content in Figures 5a–5c. And there was also a relative maximum around 2.5 km for the cloud liquid water content in Figures 5d–5f. In the maturity stage, two separated liquid layers were found at 1 and 2.5 km, respectively. The same situation also appears in previous research (Bao et al., 2016; Yao et al., 2014). We assumed that the maximum liquid water layers in 1 km were affected by the large amount of the moist air under the inversion layer. The air below the inversion exchanges momentum and moist enthalpy with the sea and mixes in complicated ways with air from the eye wall (Willoughby, 1998). With the strengthening of TCCS, there are the most ice particles ($\geq$9 g/m^3) in the high altitude and least water droplets ($\leq$6 g/m^3) in the low altitude in maturity stage. This result matches well with the $PCT_{85.5}$ distribution, which further illustrates the development of the TCCS and ice particles concentration in this stage. Meanwhile, in the decay stage, the most liquid water droplets ($\geq$40 g/m^3) and the least ice water

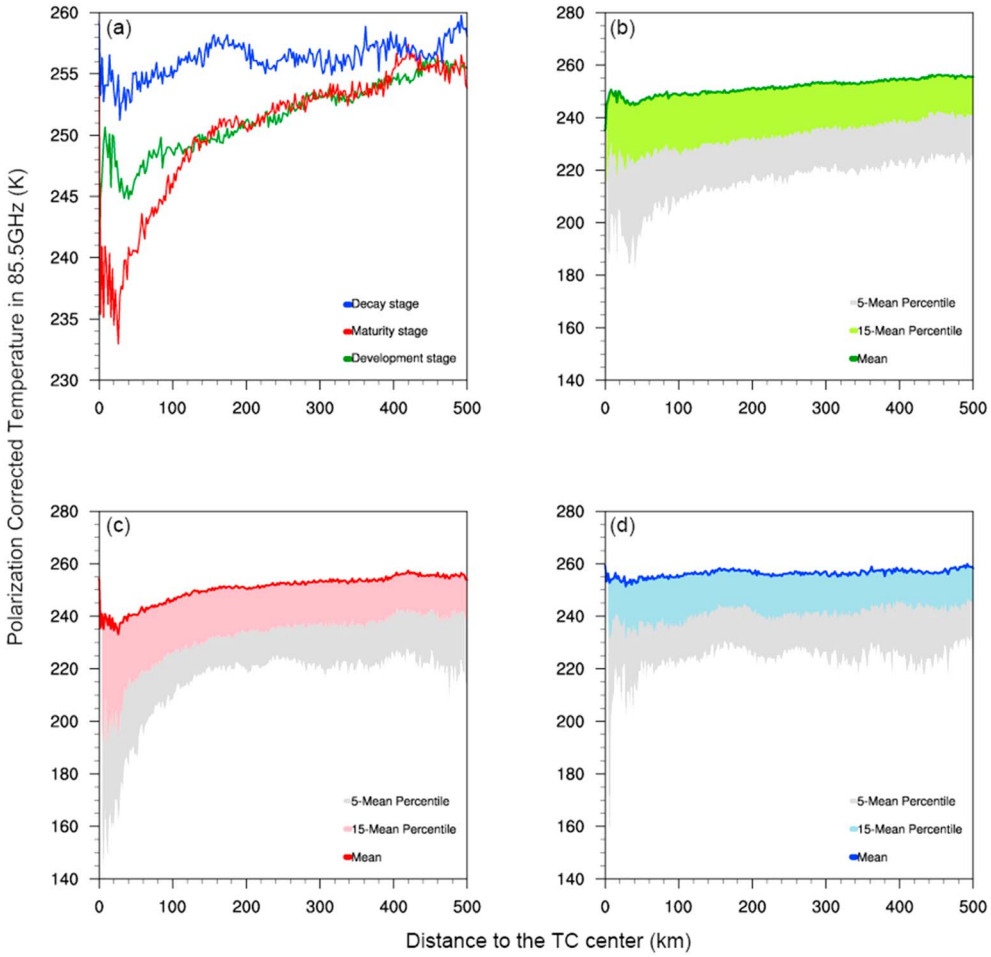

Figure 4. The $PCT_{85.5}$ radial variation is derived from Tropical Rainfall Measuring Mission 1B11 products. (a) Variations in the range of 500 km. The detail variations and $PCT_{85.5}$ distribution in (b) development stage, (c) maturity stage, (d) decay stage of TC cloud system, respectively. The gray shadow represents value of the 5–15 percentiles and the colorful shadow represents the 15-mean percentiles. TC = tropical cyclone.

particles (around 7 g/m^3) are found than those at other two stages. To some extent, the content of ice particles can reveal the genesis and extinction of the TCCS. When locating in the ocean, plenty of energy sources from the warm sea surface provide TCCS with strong updrafts. The moisture from the see surface will be taken to the high level and then convert to the ice crystal. Once TCs make landfall, the surface friction and the disappearance of energy source make the TC intensity decrease rapidly. Thus, there will be more ice crystal converting to the water droplets in this stage.

Figure 6 gives the spatial variations of COT, CWP, and CER from MODIS product along the radial direction of TC. The results indicate the formation, development, and extinction of a TC. According to the radar reflectivity calculated above, the high value (≥28 dBZ) could represent the eye wall of a TCCS. Therefore, a range of 200 km would cover the full scope of eye wall and the TCCS optical properties always have remarkable characteristics within this range. For the CWP and COT in Figures 6a and 6b, they show similar variation trend. In the maturity stage, the mean CWP and COT display a sharp increase in the TC eye wall, and then decreases rapidly out of 100 km. We can observe that there are more water droplets concentrated in the cloud top in the maturity stages. But in the development stage and decay stage, they decrease slowly with the increase of distance. The lines or values of CWP in the TC development and extinction stage are close to each other in the whole distance, while the COT value at the decay stage is significantly higher than that at the development stage. In order to model their spatial variability, we make the regression analysis as shown in the dashed lines in Figure 6.

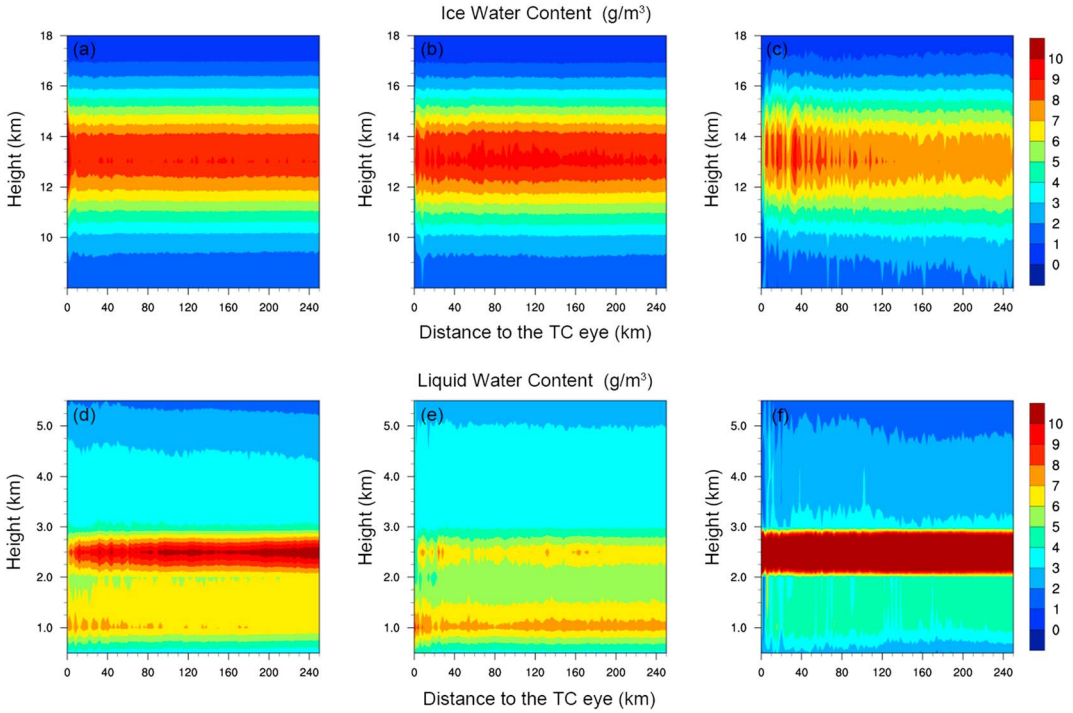

Figure 5. Height-radius sections of (a)–(c) cloud ice water content (g/m^3) and (d)–(f) cloud liquid water in the development (left), maturity (middle), and decay (right) stage of TCs, respectively. TCs = tropical cyclones.

Table 3 gives the regression results (fitting equation and R^2) about the variation trend of CWP, COT, and CER in the development, maturity, and decay stages of TCCS, respectively. In Figures 6a and 6b, the regression fitting equations for development and decay are $y = 834.658 - 1.114x$ and $y = 785.610 - 0.951x$ for CWP and $y = 43.723 - 0.061x$ and $y = 51.273 - 0.061x$ for COT, respectively. However, in the maturity stage, they exhibit a strong variation in radial direction, especially within 200 km. The greatest water concentration appears near 100-km location, where the peak values are about 1323.16 g/m^2 for CWP and 74.09 for COT. The regression equations in this stages (Figures 6a and 6b) are $y = 366.872 + \frac{35638973.050}{4(x-51.958)^2+39869.327}$ and$y = 19.619 + \frac{1890157.489}{4(x-48.548)^2+36948.402}$, respectively. The high regression R^2 (exceed 0.95) indicates that there are strong linear relationship between the two parameters (COT and CWP) and the distance. The small residual sum of squares illustrates that regression equations are greatly fitted to the observation data (The detailed information can be seen in the Table 3). However, the fitting results are not good in the vicinity of TC eye because the eye of a TC is a zone of weak winds, and the weather is normally calm and free of clouds. In addition, there are a lot of small-scale, hard-to-observe, transient convective bursts in the eye wall. The sudden change characteristics of cloud lead to great discrepancies of cloud properties in a continuous area.

As we know, the different TCCSs usually have different radial sizes. In order to achieve better optical characteristics spatial distribution of TCCSs, the results should be normalized. That is to say, for each TC, when calculating the mean cloud optical properties distribution from 0 to 500 km, the x-axis should use the radial distance divided by the mean maximum wind radius, not the radial distance. Figure 6d depicted the normalized result in the maturity stage for COT. The change trend is similar with the spatial distribution in Figure 6b. It has a peak value of 71.849 where the proportion is 0.19. After that, the COT declined rapidly. When the proportion is larger than 2.5, it fluctuated greatly again and the result has some difference compared to the spatial distribution. We propose this method to illustrate that both of them could explain the distribution of optical properties of TCCS while the only difference is the x axis. However, the distance to the TC center could clearly and directly illustrate the spatial variation of TCCS more than the proportion. In addition, the lack of the data set in the development and decay stages prevented us making further analysis, which is why we select the method of distance distribution denormalized as the x axis in this paper.

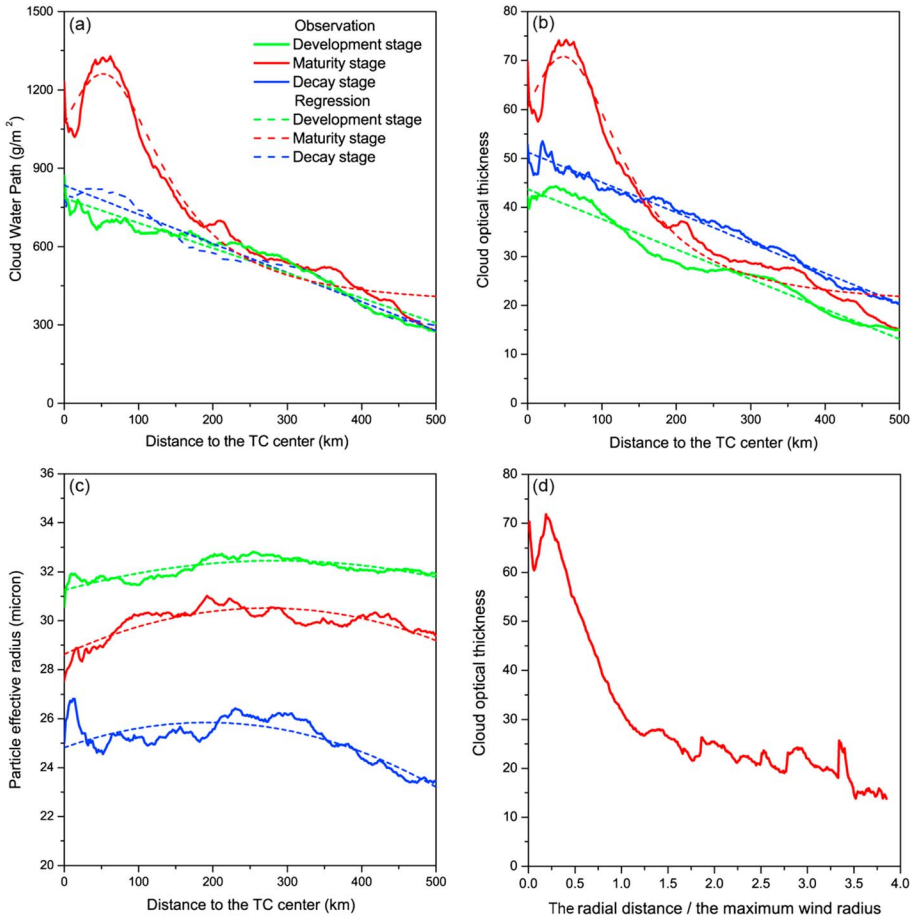

Figure 6. The radial profiles for the cloud water path (a), cloud optical thickness (b), and cloud particle effective radius (c) are derived from Moderate Resolution Imaging Spectroradiometer MOD06 products, respectively. (d) The normalized cloud optical thickness for maturity stage only. TC = tropical cyclone.

For the CER, all the regression lines are shown in Figure 6c. A very interesting feature is that no great variation can be found following the TCCS radial direction of each stage. Within the radial distance of 0–500 km, only some slight fluctuation is found for each stage. After the landfall of TCCS, the CER is close to 25 μm in the decay stage, which is smaller than the 32 μm of the development stage and 30 μm of maturity stage.

Table 3
The Regression Fitting Equation, R^2 and Residual Sum of Squares of CWP, COT, and CER in the Development, Maturity, and Decay Stages, Respectively

Stages		Regression fitting equation	R^2	Residual sum of squares
CWP	Development stage	$y = 834.658 - 1.114x$	0.969	204885.328
	Maturity stage	$y = 366.872 + \frac{35638973.050}{4(x-51.958)^2+39869.327}$	0.964	817470.369
	Decay stage	$y = 785.610 - 0.957x$	0.943	289867.360
COT	Development stage	$y = 43.723 - 0.061x$	0.963	797.436
	Maturity stage	$y = 19.619 + \frac{1890157.489}{4(x-48.548)^2+36948.402}$	0.970	2197.143
	Decay stage	$y = 51.273 - 0.061x$	0.985	306.684
CER	Development stage	$y = 31.249 + 0.008x - 0.00001x^2$	0.674	12.078
	Maturity stage	$y = 28.627 + 0.138x - 0.00003x^2$	0.687	28.901
	Decay stage	$y = 24.823 + 0.011x - 0.00003x^2$	0.671	59.676

Note. COT = cloud optical thickness; CWP = cloud water path; CER = cloud particle effective radius.

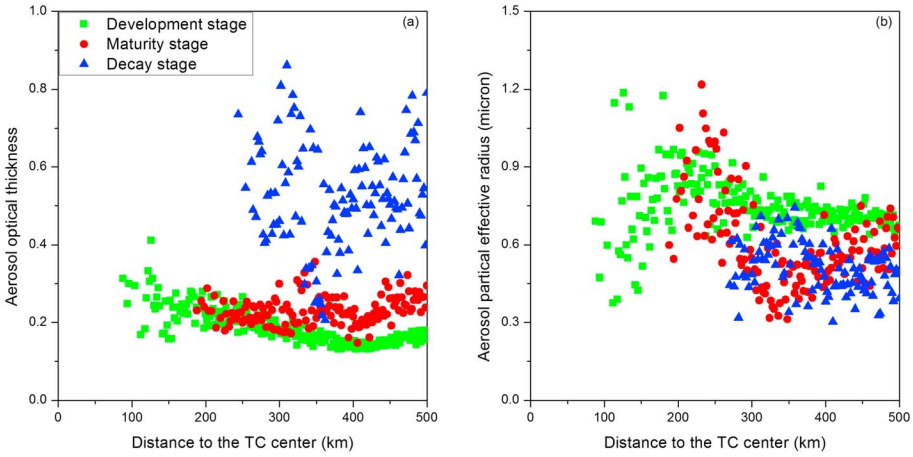

Figure 7. The variation curves for the aerosol optical thickness (a) and aerosol effective radius (b) are derived from Moderate Resolution Imaging Spectroradiometer MOD04 products. TC = tropical cyclone.

Kobayashi (2007) found that the CER for precipitation clouds is always larger than that of nonprecipitation clouds. The decrease of CER in the decay stage indicates that there is less precipitation when TC makes a landfall. Previous researches also revealed that aerosols could affect the cloud droplets (Albrecht, 1989; Bréon et al., 2002; Rosenfeld, 2000) by increasing the aerosol concentrations and decreasing the cloud drop size. From Figure 6c, the strongest stage of TCCS is not always corresponded to the largest CER, which might be associated by the aerosol concentration.

To illustrate the special change of CER, we calculate the AOT, a proxy for the aerosol concentration and effective radius (AER) around the TCCS. As we can obviously see from Figures 7a and 7b, the aerosol characteristics in the decay stage show significant difference from those in the development and maturity stages. For instance, the decrease in aerosol particle size and increase in optical thickness are indicated in the decay stage of TC; the average AOT is around 0.6 in the decay stage while in the development and maturity stage it displays near 0.2. However, the AER shows that, in the development stage, the mean effective radius is 0.3 μm larger than the one at the other two stages. From Figure 6c, we know that cloud droplet size is found to be the smallest in the decay stage which might be associated high aerosol loadings (i.e., high AOT) shown in Figure 7a. After the landfall of TC, the smaller and diverse aerosols on land may inhibit collision-coalescence in the cloud, suppressing cloud droplet growth that stops drizzle and other precipitation (Albrecht, 1989). The MODIS could not provide us with the aerosol product covered by cloud. That is to say, the MODIS aerosol observation data in the TC center is very few in the TC center and become more concentrated at the edge of TCCS.

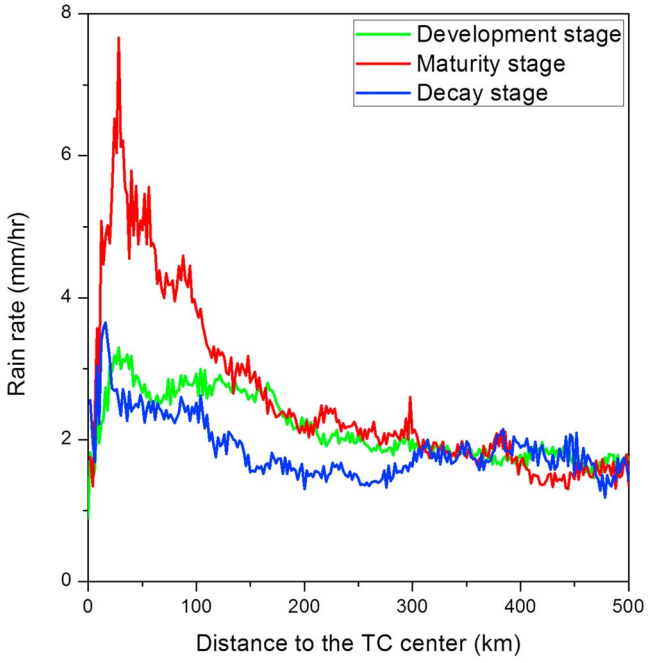

Figure 8. The integral of rain rate from the top to bottom retrieved from Tropical Rainfall Measuring Mission 2A25 product in development stage, maturity stage, and decay stage. TC = tropical cyclone.

The changes in the microphysical and optical properties of cloud and aerosol will finally alter cloud precipitation efficiency. Measurement from TRMM 2A25 product in Figure 8 shows that the highest rain rate within the 100 km in maturity stage is up to 7.68 mm/hr. It decreases sharply to near 2 mm/hr from the eye wall to the spiral-cloud band. In the development and decay stage, the precipitation in the eye wall is a little higher than the other region. When the TC becomes weaker or further away from the center (≥400 km), the rain rates in decay stage is a little higher than the other two stages.

3.3. Case Study

Herein, we make two case analysis for the Typhoon *Damrey* which originated from a tropical disturbance, southwest of Minamitorishima late on 26 July 2012. On 30 July, Damrey began to track northwestward and was

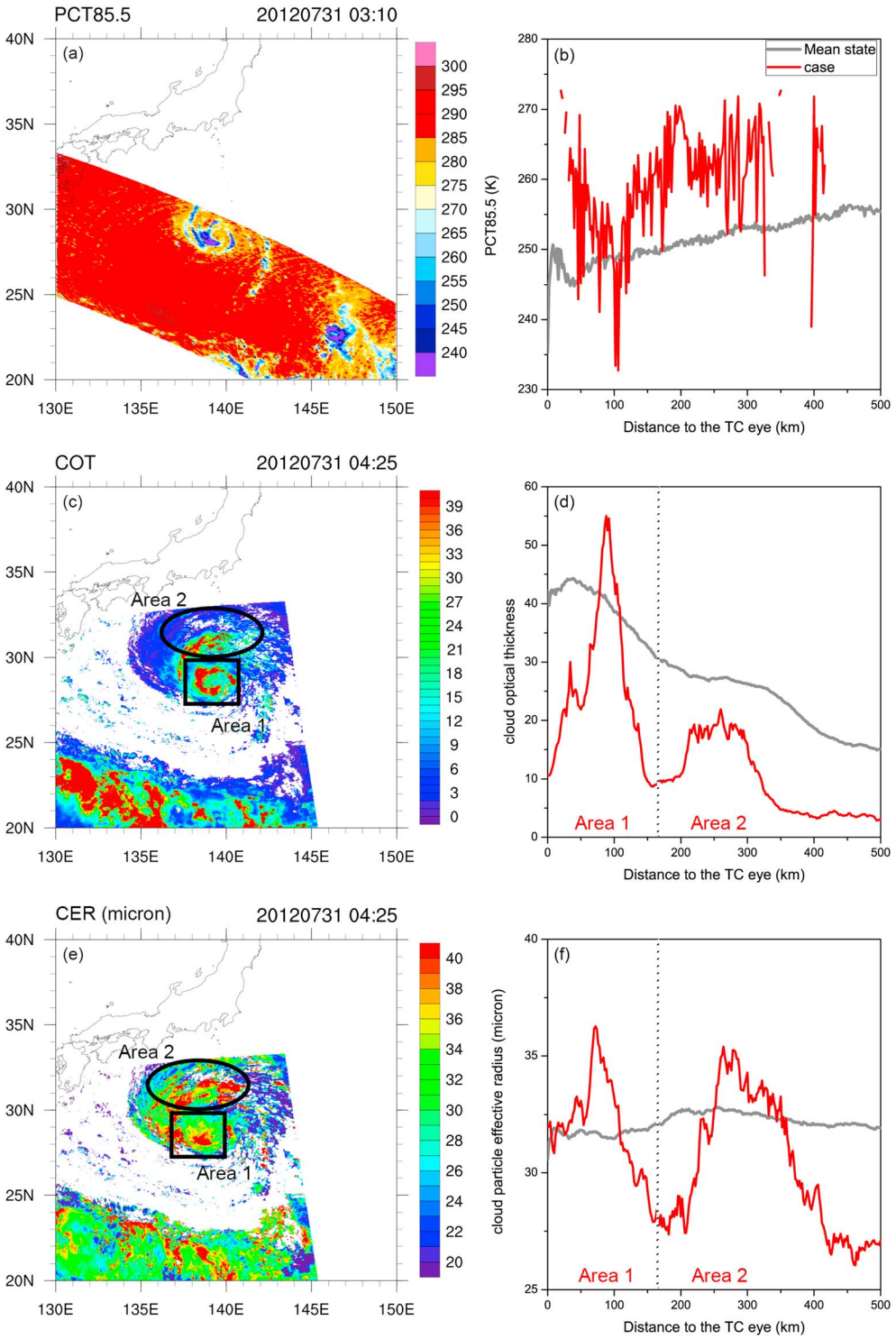

Figure 9. The imagery for $PCT_{85.5}$ (K) (a–b) derived from Tropical Rainfall Measuring Mission and COT (c–d) and CER (micron) (e–f) derived from Moderate Resolution Imaging Spectroradiometer for case 1. Their change trend within the 500 km from the TC eye is calculated and compared with the mean state in the development stage (gray line) in (b), (d), and (f), respectively. COT = cloud optical thickness; CER = cloud particle effective radius; TC = tropical cyclone.

intensified into a STS. Then, On 1 August, it tracked over the warmest region and began to weaken. In order to verify the statistical mean state above and the aerosol effect on cloud and precipitation, this case is selected. The data measured by the TRMM and MODIS were collected at 0310 and 0425 UTC on 31 July for case 1,

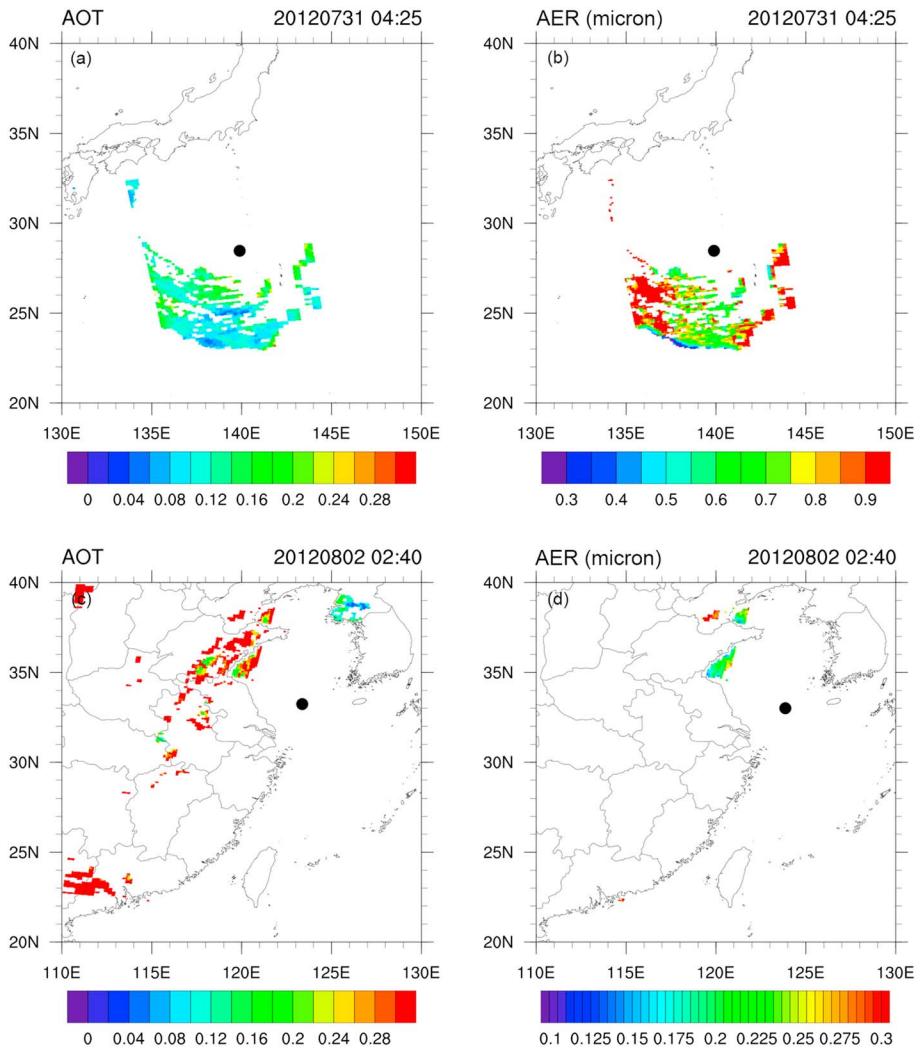

Figure 10. The AOT and AER (micron) distribution around the Damrey at 0425 UTC on 31 July (a–b) for case 1 and 0240 UTC on 2 August (c–d) for case 2 from the Moderate Resolution Imaging Spectroradiometer aerosol product (MOD04). The black dot is the location of the tropical cyclone eye at that moment. AOT = aerosol optical thickness; AER = aerosol effective radius.

which is in the development stage of Damrey, and 0115 and 0240 UTC on 2 August for case 2 in decay stage. The location of TC center is at 28.46°N and 139.89°E from the TRMM data and 28.52°N and139.45°E from the MODIS in case 1, and 33.01°N, 123.86°E and 33.24°N, 123.37°E for TRMM and MODIS in case 2, respectively.

The optical imagery serves as an important tool for the identification of the TC location and its physical characteristics. On 31 July 2012, the $PCT_{85.5}$ shows extremely low value around the TC eye (Figure 9a). When the parameters of Damrey is compared to the mean state calculated in section 3.2, the $PCT_{85.5}$ fluctuated remarkably and 10–20 K higher (Figure 9b). In the eye wall region for Damrey, the $PCT_{85.5}$ shows a modest decline and soon increases from 100 to 200 km. The maps of the retrieved COT and CER are given in Figures 9c and 9e. From Figure 9, we can clearly see that the vast majority of the cloud is located in the northern side of the TCCS. The COT around the TC periphery at this moment is under 12 and most of the cloud droplets size in this region is smaller than 30 μm. There are two maximum centers both for COT and CER. One area is around the TC center (Area 1) and another is in the north of the TC center (Area 2) (Figures 9c and 9e). The calculated change trend from the TC eye to the spiral-cloud rain band can also show the cloud variation characteristic for Damrey (Figures 9d and 9f). The results show two peaks, the first one is near the 100 km where the most active convective system occurs. Within this range, the COT and CER can reach up to 54.58 and

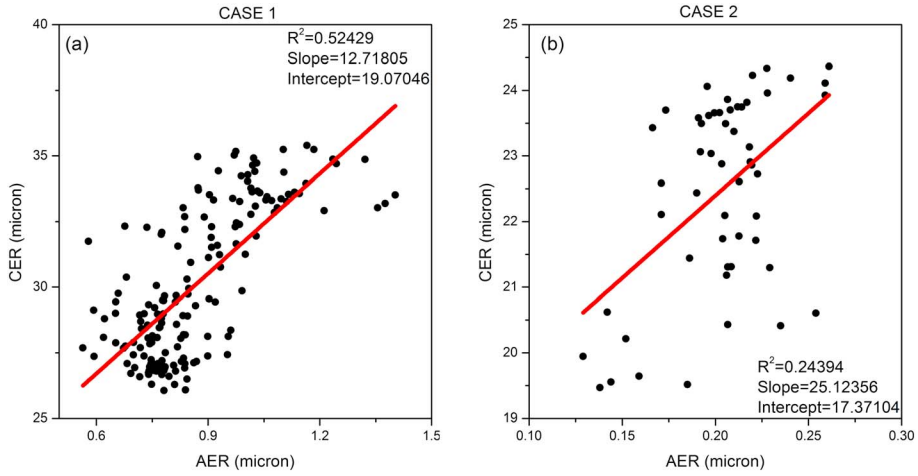

Figure 11. Correlations between AER and CER for (a) case 1 and (b) case 2 of tropical cyclone *Damrey*, respectively. AER = aerosol effective radius; CER = cloud particle effective radius.

36.26 μm, respectively. The second one is between the ranges of 250–300 km, which is consistent to the spiral-cloud band northern of the center eye. Although the COT is much lower than the first peak, they have almost the same CER in this region. By comparison with the case of TC Damrey, we found that the single case fluctuated around the mean state and the deviation was acceptable.

Figure 10 presents the average AOT and AER map derived from MODIS MOD 04 product along the track of TC. The product which cover the domain of the TCCS shows that, when the TC is far away from the continent (Figures 10a and 10b), AOT is 0–0.2 around the TCCS and AER is larger than 0.5 μm. Once the TC begins to move closely to the continent (Figures 10c and 10d), the AOT increased larger than 0.3 significantly. However, compared to case 1, the AER in case 2 has a dramatic decline, which varies in the range of 0.15–0.25 μm. Previous section has shown that the AOT is much higher, while AER is much smaller in the decay stage than those in the development and maturity stage. The distribution of the AOT and AER in this case is consistent with the statistical results.

Cloud microphysical properties can intrinsically link to the characteristics of aerosols. Increasing aerosol number concentration is hypothesized to prevent the cloud droplet coalescence. In the premise of that we have presented the spatial distribution of AOT and AER, the correlation between them is calculated when they have the same distance to the TC eye. A much stronger positive correlation coefficient of 0.524 for AER and CER in case 1 and 0.244 for case 2 is shown (Figure 11). From Figures 6c and 7b, we can see that the decay

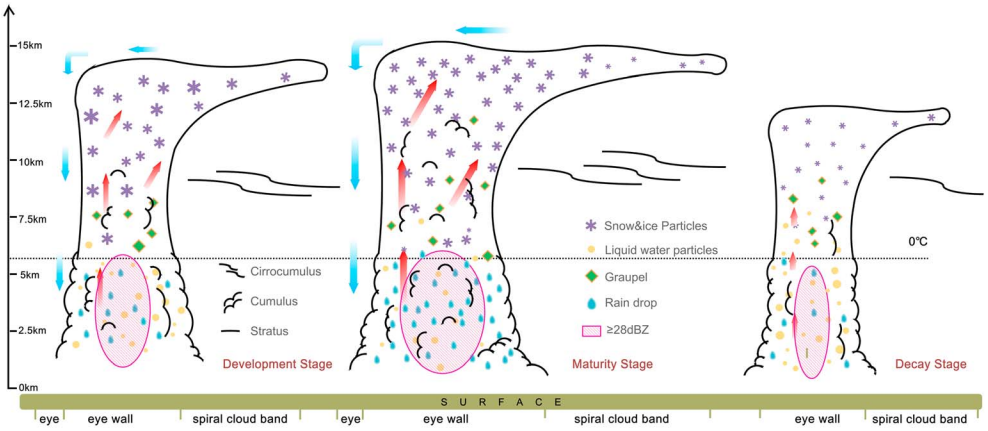

Figure 12. The scheme depiction of tropical cyclone cloud system at the development, maturity, and decay stages, respectively.

stage has the smallest CER and AER, while the development stage has the largest CER and AER. The cloud liquid water content in Figures 5d and 5f suggests that the decay stage has more water vapor content than that of development stage. Cloud droplet formation depends on the condensation of water vapor on ambient aerosols (Raatikainen et al., 2013). That is to say, a larger supersaturation activates more aerosols, resulting in numerous smaller cloud droplets. The more water vapor exists near the aerosol, the more cloud droplets will form and the smaller the droplets size will be. Therefore, a strong correlation is found between CER and AER.

4. Conclusion and Summary

In this study, we have analyzed the 5-year of the TRMM and MODIS retrievals to characterize the spatial structure and optical properties of TCCS in East Asia, in the years of 2010–2014. The spatial variability of the TCCS at the three stages (development, maturity, and decay stages) is presented which include the radar reflectivity, $PCT_{85.5}$, CWP, COT, and CER.

The results indicate that the cloud properties have noticeable characteristics in the maturity stage for the most of the parameters. We found that the TC cloud spectrum had a close connection with the cloud structure. The extremely high value of radar reflectivity usually occurs with strong updraft and convective activity, particularly in the maturity stage. The $PCT_{85.5}$ and hydrometeor profiles can reflect the amount of ice particles contained in the top of the TCCS. With the strengthening TCs, there are more ice particles accumulated on the top of cloud, especially in the TC cloud eye wall, which bring down $PCT_{85.5}$ there. Simultaneously, in the maturity stage, the statistical results also indicate the biggest COT and CWP. The peaks of $PCT_{85.5}$, COT, CWP, and radar reflectivity occur in the cloud eye wall. However, CER shows a small fluctuation along the whole distance from the eye wall and the maximum value in the decay stage, which might be associated with the precipitation and aerosol concentration. Therefore, to investigate the hypothesis, we calculated the AOT, AER, and the precipitation. The aerosol characteristics in the decay stage have significant difference from those in the development and maturity stages. In this stage, the AOT is larger whereas the AER becomes smaller and the precipitation becomes weaker. So the microphysical process and the aerosol indirect effect on the clouds and rain rate can be illustrated clearly.

Based on these observed results, several ideal fitting equations were constructed to characterize the variability of TCCS along the radial distance from the TC center. This will help promote the initial field data assimilation in numerical weather prediction.

In this paper, our emphasis has been placed on the quantification of TCCS from the remote sensing data set. This study would help quantify the optical characteristics near the top of TC that are crucial to the prediction of TC intensity and precipitation. The distribution of cloud optical properties is essential for the characterizing of global atmospheric hydrology. From the vertical profiles of TCCS retrieved, we construct an ideal conceptual model to provide a quantitative view of TCCS in each stage. Assuming that TCCS is a symmetric system, a simplified depiction for TCCS cross section in different stages is given (see Figure 12). As we know, TC is a warm-core low pressure systems associated with a spiral inflow of mass at the bottom level. The spiral outflow at the top level is vertical motion, and the TC clouds are usually dominated by the open eye of the storm, central convective eye region, and spiraling cirrostratus outward horizontally. The symmetric structure of TCCS is usually destroyed by the disappearance of the eye and the spiral cloud in the decay stage. From the microphysical view, the particle size, phase, and distributions exhibit a wide variety in radial and vertical direction. According to the statistical analysis above, there are more ice particles in the maturity stage, and the liquid water becomes more in the decay stage. We note that the ideal model we constructed here simplifies the TCCS and defines the structure and optical characteristics in a symmetric cloud system (see Figure 12). However, it can depict the moisture transition inside the TCCS during the time period of genesis and extinction of a TC. These physical quantities are studied through the preceding part of the text. The ideal conceptual model can help us understand the distribution of optical properties on TCCS in statistics. If the model can be optimized, it can be executed on a large-scale TC environment and different forms of output can be produced.

Finally, two cases for the TC Damrey were studied. The result was compared with the statistical average, and we found the example of Damrey influenced by less raw data and high fluctuation, but the tendency of the

cloud parameters has been denoted well with expectation. Damrey's eye wall usually has many prominent characteristics, such as a thicker COT, larger CER, and a sharp decreasing $PCT_{85.5}$. Enhanced aerosol concentrations can suppress warm-rain processes by reducing particle sizes and thereby cause a narrow droplet spectrum. A strong correlation was also found between CER and AER influenced by the water vapor. The aerosol indirect effect has been demonstrated that aerosol have a large influence on the cloud condensation nuclei and modify the cloud properties.

The results presented in this study are useful for evaluating numerical simulations for TC prediction. In addition, the importance of quantifying the indirect effect on clouds to minimize the uncertainty in the aerosol-cloud interaction has been emphasized. Future work will explore the effect of the atmospheric boundary layer structure by TC using the satellites and meteorological profile data.

Acknowledgments

This work was jointly supported by the National Key R&D Program of China Project (Grant # 2016YFC0203303), the Jiangsu Natural Science Foundation Provence (Grant # BE2015151), and the National Natural Science Foundation of China (NSFC#; Grant # 41775026, 41075012, 40805006, and 91544230). Special thanks to Ms. Anjeza Arapi, a native English-speaking person, who comes from NOAA-CREST, City College of the City University of New York, for helping us to polish the English language usage of this article. And the authors also would like to thank the two anonymous reviewers for their valuable comments and suggestions, which will greatly help to improve the quality of this article. All the data used are listed in the references or archived in repository as follows: the TRMM data can be obtained from the Goddard Space Flight Center at NASA from https://trmm.gsfc.nasa.gov/, the MODIS data are provided by NASA through the website https://modis.gsfc.nasa.gov/data/, the 35 TCs landing in China from 2010 to 2014 can be found from the RSMC Tokyo-Typhoon Center website http://www.jma.go.jp/, and the intensity classification standard can be found from China Meteorology Administration website http://tcdata.typhoon.gov.cn.

References

Albrecht, B. A. (1989). Aerosols, cloud microphysics, and fractional cloudiness. *Science*, *245*(4923), 1227–1230. https://doi.org/10.1126/science.245.4923.1227

Balaguru, K., Taraphdar, S., Leung, L. R., Foltz, G. R., & Knaff, J. A. (2014). Cyclone-cyclone interactions through the ocean pathway. *Geophysical Research Letters*, *41*, 6855–6862. https://doi.org/10.1002/2014GL061489

Bao, J. W., Michelson, S. A., & Grell, E. D. (2016). Pathways to the production of precipitating hydrometeors and tropical cyclone development. *Monthly Weather Review*, *144*(6), 2395–2420. https://doi.org/10.1175/MWR-D-15-0363.1

Bennartz, R. (2007). Global assessment of marine boundary layer cloud droplet number concentration from satellite. *Journal of Geophysical Research*, *112*, D02201. https://doi.org/10.1029/2006JD007547

Boeke, R. C., Allan, A. M., & Coakley, J. A. Jr. (2016). Properties of marine stratocumulus obtained with partly cloudy pixel retrievals and found in the MODIS MOD06 cloud product. *Journal of Geophysical Research: Atmospheres*, *121*, 6404–6424. https://doi.org/10.1002/2015JD024149

Bréon, F. M., Tanré, D., & Generoso, S. (2002). Aerosol effect on cloud droplet size monitored from satellite. *Science*, *295*(5556), 834–838. https://doi.org/10.1126/science.1066434

Chan, J. C., & Kepert, J. D. (2010). *Global perspectives on tropical cyclones: From science to mitigation* (Vol. 4, p. 436). World Scientific Publishing Co, Inc. https://doi.org/10.1142/7597

Chang, C.-P., Lei, Y., Sui, C.-H., Lin, X., & Ren, F. (2012). Tropical cyclone and extreme rainfall trends in East Asian summer monsoon since mid-20th century. *Geophysical Research Letters*, *39*, L18702. https://doi.org/10.1029/2012GL052945

Chao, C., Liu, G., & Liu, C. (2011). Estimation of the upper-layer rotation and maximum wind speed of tropical cyclones via satellite imagery. *Journal of Applied Meteorology and Climatology*, *50*(3), 750–766. https://doi.org/10.1175/2010JAMC2519.1

Chen, S. S., Knaff, J. A., & Marks, F. D. Jr. (2006). Effects of vertical wind shear and storm motion on tropical cyclone rainfall asymmetries deduced from TRMM. *Monthly Weather Review*, *134*(11), 3190–3208. https://doi.org/10.1175/MWR3245.1

Durden, S. L., Tanelli, S., & Dobrowalski, G. (2009). CloudSat and A-Train observations of tropical cyclones. *Open Atmospheric Science Journal*, *3*(1), 80–92. https://doi.org/10.2174/1874282300903010080

Englehart, P. J., & Douglas, A. V. (2001). The role of eastern North Pacific tropical storms in the rainfall climatology of western Mexico. *International Journal of Climatology*, *21*(11), 1357–1370. https://doi.org/10.1002/joc.637

Haig, J. E.-A., & Nott, J. (2016). Solar forcing over the last 1500 years and Australian tropical cyclone activity. *Geophysical Research Letters*, *43*, 2843–2850. https://doi.org/10.1002/2016GL068012

Han, H., Li, J., Goldberg, M., Wang, P., Li, J., Li, Z., et al. (2016). Microwave sounder cloud detection using a collocated high-resolution imager and its impact on radiance assimilation in tropical cyclone forecasts. *Monthly Weather Review*, *144*(10), 3937–3959. https://doi.org/10.1175/MWR-D-15-0300.1

Han, Q., Rossow, W. B., Chou, J., & Welch, R. M. (1998). Global survey of the relationships of cloud albedo and liquid water path with droplet size using ISCCP. *Journal of Climate*, *11*(7), 1516–1528. https://doi.org/10.1175/1520-0442(1998)011<1516:GSOTRO>2.0.CO;2

Heinselman, P. L., Stensrud, D. J., Hluchan, R. M., Spencer, P. L., Burke, P. C., & Elmore, K. L. (2009). Radar reflectivity-based estimates of mixed layer depth. *Journal of Atmospheric and Oceanic Technology*, *26*(2), 229–239. https://doi.org/10.1175/2008JTECHA1091.1

Heymsfield, G. M., Geerts, B., & Tian, L. (1999). TRMM precipitation radar reflectivity profiles as compared with high-resolution airborne and ground-based radar measurements. *Journal of Applied Meteorology*, *39*(12), 2080–2102. https://doi.org/10.1175/1520-0450(2001)040<2080:TPRRPA>2.0.CO;2

Houze, R. A. (2010). Clouds in tropical cyclones. *Monthly Weather Review*, *138*(2), 293–344. https://doi.org/10.1175/2009MWR2989.1

Ichoku, C., Kaufman, Y. J., Remer, L. A., & Levy, R. (2004). Global aerosol remote sensing from MODIS. *Advances in Space Research*, *34*(4), 820–827. https://doi.org/10.1016/j.asr.2003.07.071

Iguchi, T., Kozu, T., Meneghini, R., Awaka, J., & Okamoto, K. (2000). Rain-Profiling Algorithm for the TRMM Precipitation Radar. *Journal of Applied Meteorology*, *39*(12), 2038–2052. https://doi.org/10.1175/1520-0450(2001)040<2038:RPAFTT>2.0.CO;2

Kahn, R. A., Garay, M. J., Nelson, D. L., Yau, K. K., Bull, M. A., Gaitley, B. J., et al. (2007). Satellite-derived aerosol optical depth over dark water from MISR and MODIS: Comparisons with AERONET and implications for climatological studies. *Journal of Geophysical Research*, *112*(D18), D18205. https://doi.org/10.1029/2006JD008175

Kidder, S. Q., Gray, W. M., & Vonder Haar, T. H. (2009). Estimating tropical cyclone central pressure and outer winds from satellite microwave data. *Monthly Weather Review*, *106*(10), 1458–1464. https://doi.org/10.1175/1520-0493(1978)106<1458:ETCCPA>2.0.CO;2

King, M., Platnick, S., Yang, P., Arnold, G., Gray, M., Riedi, J., et al. (2004). Remote sensing of liquid water and ice cloud optical thickness and effective radius in the Arctic: Application of airborne multispectral MAS data. *Journal of Atmospheric and Oceanic Technology*, *21*(6), 857–875. https://doi.org/10.1175/1520-0426(2004)021<0857:RSOLWA>2.0.CO;2

Knapp, K. R., & Kossin, J. P. (2007). New global tropical cyclone data from ISCCP B1 geostationary satellite observations. *Journal of Applied Remote Sensing*, *1*, 013505. https://doi.org/10.1117/1.271281

Kobayashi, T. (2007). Significant differences in the cloud droplet effective radius between nonprecipitating and precipitating clouds. *Geophysical Research Letters*, *34*, L15811. https://doi.org/10.1029/2007GL029606

Koh, T., & Fonseca, R. (2015). Subgrid-scale cloud–radiation feedback for the Betts–Miller–Janjić convection scheme. *Quarterly Journal of the Royal Meteorological Society*, *142*(695), 989–1006. https://doi.org/10.1002/qj.2702

Kummerow, C. (2000). The status of the Tropical Rainfall Measuring Mission (TRMM) after two years in orbit. *Journal of Applied Meteorology*, *39*(12), 1965–1982. https://doi.org/10.1175/1520-0450(2001)040<1965:TSOTTR>2.0.CO;2

Larson, J., Zhou, Y., & Higgins, R. W. (2005). Characteristics of landfalling tropical cyclones in the United States and Mexico: climatology and interannual variability. *Journal of Climate*, *18*(8), 1247–1262. https://doi.org/10.1175/JCLI3317.1

Lau, K.-M., Zhou, Y. P., & Wu, H.-T. (2008). Have tropical cyclones been feeding more extreme rainfall? *Journal of Geophysical Research*, *113*(D23), D23113. https://doi.org/10.1029/2008JD009963

Li, T., Kwon, M., Zhao, M., Kug, J.-S., Luo, J.-J., & Yu, W. (2010). Global warming shifts Pacific tropical cyclone location. *Geophysical Research Letters*, *37*, L21804. https://doi.org/10.1029/2010GL045124

Li, Z., Niu, F., Fan, J., Liu, Y., Rosenfeld, D., & Ding, Y. (2011). Long-term impacts of aerosols on the vertical development of clouds and precipitation. *Nature Geoscience*, *4*(12), 888–894. https://doi.org/10.1038/NGEO1313

Li, Z., Niu, F., Lee, K.-H., Xin, J., Hao, W.-M., Nordgren, B., et al. (2007). Validation and understanding of Moderate Resolution Imaging Spectroradiometer aerosol products (C5) using ground-based measurements from the handheld Sun photometer network in China. *Journal of Geophysical Research*, *112*(D22), D22S07. https://doi.org/10.1029/2007JD008479

Li, Z., Zhao, F., Liu, J., Jiang, M., Zhao, C., & Cribb, M. (2014). Opposite effects of absorbing aerosols on the retrievals of cloud optical depth from spaceborne and ground-based measurements. *Journal of Geophysical Research: Atmospheres*, *119*(9), 5104–5114. https://doi.org/10.1002/2013JD021053

Lin, Y., Min, Q., Zhuang, G., Wang, Z., Gong, W., & Li, R. (2010). Spatial features of rain frequency change and pollution and associated aerosols. *Atmospheric Chemistry and Physics*, *9*(1), 3555–3762. https://doi.org/10.5194/acpd-9-3555-2009

Liu, C., Zipser, E., Cecil, D., Nesbitt, S., & Sherwood, S. (2008). A cloud and precipitation feature database from nine years of TRMM observations. *Journal of Applied Meteorology and Climatology*, *47*(10), 2712–2728. https://doi.org/10.1175/2008JAMC1890.1

Lu, X. Q., Yu, H., & Lei, X. T. (2011). Statistics for size and radial wind profile of tropical cyclones in the western north pacific. *Journal of Meteorological Research*, *25*(1), 104–112. https://doi.org/10.1007/s13351-011-0008-9

Marchand, R., Ackerman, T., Smyth, M., & Rossow, W. B. (2010). A review of cloud top height and optical depth histograms from MISR, ISCCP, and MODIS. *Journal of Geophysical Research*, *115*(D16), D16206. https://doi.org/10.1029/2009JD013422

Martins, J. V., Tanré, D., Remer, L., Kaufman, Y., Mattoo, S., & Levy, R. (2002). MODIS cloud screening for remote sensing of aerosols over oceans using spatial variability. *Geophysical Research Letters*, *29*(12), 8009. https://doi.org/10.1029/2001GL013252

Matveev, Y. L. (1999). Dynamic and statistical analysis of global cloud fields from satellite data. *Earth Observation & Remote Sensing*, *15*(1), 115–127.

Mei, W., Primeau, F., McWilliams, J. C., & Pasquero, C. (2013). Sea surface height evidence for long-term warming effects of tropical cyclones on the ocean. *Proceedings of the National Academy of Sciences of the United States of America*, *110*(38), 15207–15210. https://doi.org/10.1073/pnas.1306753110

Menzel, W. P., Frey, R. A., & Baum, B. A. (2015). Cloud top properties and cloud phase algorithm theoretical basis document, Version 11. [Available at http://modis-atmos.gsfc.nasa.gov/_docs/MOD35_ATBD_Collection6.pdf.].

Min, Q., Joseph, E., Lin, Y., Min, L., Yin, B., Daum, P. H., et al. (2012). Comparison of MODIS cloud microphysical properties with in-situ measurements over the Southeast Pacific. *Atmospheric Chemistry and Physics*, *12*(23), 11261–11273. https://doi.org/10.5194/acp-12-11261-2012

Min, Q. L., Li, R., Lin, B., & Joseph, E. (2008). Evidence of mineral dust altering cloud microphysics and precipitation. *Atmospheric Chemistry and Physics*, *9*(9), 3223–3231. https://doi.org/10.5194/acp-9-3223-2009

Montgomery, M., & Farrell, B. (1993). Tropical cyclone formation. *Journal of the Atmospheric Sciences*, *50*(2), 285–310. https://doi.org/10.1175/1520-0469(1993)050<0285:TCF>2.0.CO;2

Nakajima, T., & King, M. (1990). Determination of the optical thickness and effective particle radius of clouds from reflected solar radiation measurements. Part I: Theory. *Journal of the Atmospheric Sciences*, *47*(15), 1878–1893. https://doi.org/10.1175/1520-0469(1990)047<1878:DOTOTA>2.0.CO;2

Nesbitt, S. W., Zipser, E. J., & Cecil, D. J. (1999). A census of precipitation features in the tropics using TRMM: Radar, ice scattering, and lightning observations. *Journal of Climate*, *13*(23), 4087–4106. https://doi.org/10.1175/1520-0442(2000)013<4087:ACOPFI>2.0.CO;2

Olson, E., Zipser, E., Smith, T., Wilheit, G., North, T., Krishnamurti, T., & Nakamura, K. (2000). The status of the Tropical Rainfall Measuring Mission (TRMM) after two years in orbit. *Journal of Applied Meteorology*, *39*(12), 1965–1982. https://doi.org/10.1175/1520-0450(2001)040<1965:TSOTTR>2.0.CO;2

Otkin, J. A., & Greenwald, T. J. (2008). Comparison of WRF model-simulated and MODIS-derived cloud data. *Monthly Weather Review*, *136*(6), 1957–1970. https://doi.org/10.1175/2007MWR2293.1

Pithan, F., Medeiros, B., & Mauritsen, T. (2014). Mixed-phase clouds cause climate model biases in arctic wintertime temperature inversions. *Climate Dynamics*, *22*(1), 13–31. https://doi.org/10.1007/s00382-003-0365-x

Platnick, S., King, M. D., Ackerman, S. A., & Menzel, W. P. (2003). The MODIS cloud products: Algorithms and examples from Terra. *IEEE Transactions on Geoscience and Remote Sensing*, *41*(2), 459–473. https://doi.org/10.1109/TGRS.2002.808301

Platnick, S., K. G. Meyer, M. D. King, G. Wind, N. D. Amarasinghe, B. Marchant et al. (2015). MODIS cloud optical properties: User guide for collection 6 level-2 MOD06/MYD06 product and associated level-3 datasets. Retrieved from http://modis-tmos.gsfc.nasa.gov/_docs/C6MOD06 OPUserGuide.pdf

Raatikainen, T., Nenes, A., Seinfeld, J. H., Morales, R., Moore, R. H., Lathem, T. L., et al. (2013). Constraining the water vapor uptake coefficient in ambient cloud droplet formation. In *AIP* (Vol. 1527, pp. 812–816). Fort Collins, CO: American Institute of Physics. https://doi.org/10.1063/1.4803395

Redemann, J., Zhang, Q., Russell, P. B., Livingston, J. M., & Remer, L. A. (2009). Case studies of aerosol remote sensing in the vicinity of clouds. *Journal of Geophysical Research*, *114*(D6), D06209. https://doi.org/10.1029/2008JD010774

Rosenfeld, D. (2000). Suppression of rain and snow by urban and industrial air pollution. *Science*, *287*(5459), 1793–1796. https://doi.org/10.1126/science.287.5459.1793

Rosenfeld, D., Woodley, W. L., Khain, A., Cotton, W. R., Carrió, G., Ginis, I., & Golden, J. H. (2012). Aerosol effects on microstructure and intensity of tropical cyclones. *Bulletin of the American Meteorological Society*, *93*(7), 987–1001. https://doi.org/10.1175/BAMS-D-11-00147.1

Spencer, R., Goodman, H., & Hood, R. (1989). Precipitation retrieval over land and ocean with the SSM/I: Identification and characteristics of the scattering signal. *Journal of Atmospheric and Oceanic Technology*, *6*(2), 254–273. https://doi.org/10.1175/1520-0426(1989)006<0254:PROLAO>2.0.CO;2

Squires, P., & Twomey, S. (1960). The relation between cloud droplet spectra and the spectrum of cloud nuclei. *Physics of Precipitation*: Proceedings of the Cloud Physics Conference, Woods Hole, Massachusetts, June 3–5, 1959, American Geophysical Union, 1960: 211–219. https://doi.org/10.1029/GM005p0211

Sriver, R. L., & Huber, M. (2007). Observational evidence for an ocean heat pump induced by tropical cyclones. *Nature*, *447*(7144), 577–580. https://doi.org/10.1038/nature05785

Stephens, G. L., & Wong, T. (1987). The effects of clouds on climate as deduced from simple models. In *Atmospheric radiation* (pp. 418–425). Boston, MA: American Meteorological Society. https://doi.org/10.1007/978-1-935704-18-8_62

Szczodrak, M., Austin, P., & Krummel, P. (2001). Variability of optical depth and effective radius in marine stratocumulus clouds. *Journal of the Atmospheric Sciences*, *58*(19), 2912–2926. https://doi.org/10.1175/1520-0469(2001)058<2912:VOODAE>2.0.CO;2

Tourville, N., Stephens, G., Demaria, M., & Vane, D. (2015). Remote sensing of tropical cyclones: Observations from cloudSat and A-Train profilers. *Bulletin of the American Meteorological Society*, *96*(4), 609–622. https://doi.org/10.1175/BAMS-D-13-00282.1

Wang, Y., Fu, Y., Fang, X., & Zhang, Y. (2014). Estimating ice water path in tropical cyclones with multispectral microwave data from the FY-3B satellite. *IEEE Transactions on Geoscience and Remote Sensing*, *52*(9), 5548–5557. https://doi.org/10.1109/TGRS.2013.2290320

Wang, Y., Lee, K. H., Lin, Y., Levy, M., & Zhang, R. (2014). Distinct effects of anthropogenic aerosols on tropical cyclones. *Nature Climate Change*, *3*(2), 171–373. https://doi.org/10.1038/nclimate1811

Wang, Y., Wan, Q., Meng, W., Liao, F., Tan, H., & Zhang, R. (2011). Long-term impacts of aerosols on precipitation and lightning over the Pearl River Delta megacity area in China. *Atmospheric Chemistry and Physics*, *11*(23), 12421–12436. https://doi.org/10.5194/acp-11-12421-2011

Willoughby, H. E. (1998). Tropical cyclone eye thermodynamics. *Monthly Weather Review*, *126*(12), 3053–3067. https://doi.org/10.1175/1520-0493(1998)126<3053:TCET>2.0.CO;2

Wing, A. A., Emanuel, K., & Solomon, S. (2015). On the factors affecting trends and variability in tropical cyclone potential intensity. *Geophysical Research Letters*, *42*, 8669–8677. https://doi.org/10.1002/2015GL066145

Wood, R., Comstock, K. K., Bretherton, C. S., Cornish, C., Tomlinson, J., Collins, D. R., & Fairall, C. (2008). Open cellular structure in marine stratocumulus sheets. *Journal of Geophysical Research*, *113*(D12), D12207. https://doi.org/10.1029/2007JD009371

Yao, X., Li, W., & Chen, S. (2014). Research on latent heat distributions in tropical cyclones from hydrometeor TMI retrieval data. *Chinese Journal of Atmospheric Sciences*, *38*, 909–923. https://doi.org/10.3878/j.issn.1006-9895.1401.13188

Ying, M., Zhang, W., Yu, H., Lu, X., Feng, J., Fan, Y., et al. (2014). An overview of the China Meteorological Administration tropical cyclone database. *Journal of Atmospheric and Oceanic Technology*, *31*(2), 287–301. https://doi.org/10.1175/JTECH-D-12-00119.1

Yokoyama, C., & Takayabu, Y. N. (2008). A statistical study on rain characteristics of tropical cyclones using TRMM satellite data. *Monthly Weather Review*, *136*(10), 3848–3862. https://doi.org/10.1175/2008MWR2408.1

Yonekura, E., & Hall, T. (2014). ENSO effect on East Asian tropical cyclone landfall via changes in tracks and genesis in a statistical model. *Journal of Applied Meteorology and Climatology*, *53*(2), 406–420. https://doi.org/10.1175/JAMC-D-12-0240.1

Zhang, J., & Reid, J. S. (2006). MODIS aerosol product analysis for data assimilation: Assessment of over-ocean level 2 aerosol optical thickness retrievals. *Journal of Geophysical Research*, *111*(D22), D22207. https://doi.org/10.1029/2005JD006898